ADVANCED FUNCTIONAL MATERIALS
www.afm-journal.de

Ion-Impregnated Intermediate Layer for Enhancing Triboelectric Nanogenerator Performance

Dong Un Lim, Eun Jung Lee, Jung Kyu Jang, Sohee Kim, Su Yeon Lee, and Tae-Ho Kim**

The triboelectric nanogenerator (TENG) is gaining recognition as a highly promising, eco-friendly self-powered device for the growth of the Internet of Things (IoT). To improve the performance of TENGs, diverse materials are employed as interlayers. However, challenges related to cost and stability persist. Herein, a strategy that incorporates ion-containing electrolyte polymers as interlayers is presented. This approach effectively mitigates charge decay and maximizes TENG efficiency by leveraging the high charge capacitance of the ionic electric double layer (iEDL). The incorporation of iEDL into TENG results in an approximate tenfold increase in current density (10–92 mA m^{-2}) and a 13-fold increase in power density (2–26 W m^{-2}). The robust energy generation capabilities of iEDL-TENG enable the operation of 100 LED lights and the charging of a 470 µF capacitor. Furthermore, the demonstrated device exhibits significant stability across 10,000 operational cycles and effectively maintains its performance when subjected to external physical forces such as blade-induced cuts, penetrating wounds, and severe crumpling.

1. Introduction

The integration of the Internet of Things (IoT) has ushered in new possibilities for creating intelligent environments and transforming our interactions with the world. However, a persistent crucial challenge lies in providing a constant supply of energy to the sensor networks distributed among countless objects in the IoT ecosystem. Instead of relying on external power sources such as batteries, self-powered systems can be a preferable alternative. In this regard, TENG stands out as one of the most noteworthy energy harvesting technologies. TENG, initially demonstrated by Wang's group in 2012,[1] is a device that enables the conversion of mechanical energy into electrical energy.[2] It is highly regarded as an eco-friendly, self-powered device for IoT system sensors, offering simplicity and convenience in operation.[3]

The successful deployment of TENG in practical applications heavily hinges on its ability to generate adequate amounts of output power. Previous efforts to boost TENG output performance have primarily focused on effectively generating triboelectric charges. These efforts included improving material performance and optimizing contact efficiency.[4] However, in conventional TENG structures, triboelectric charge decay occurs via drift or diffusion in an electric field induced by an electron concentration gradient.[5] To address this, structures aimed at reducing charge decay through the incorporation of intermediate layers have surged as promising approach in recent years[6] The charge-trapping layers typically consist of polymers and 2D materials that possess inherent physical and chemical defects, including impurities and free volume within amorphous regions, residual polar groups or other functional groups, and band gap modification.[7,8] The charge-blocking layer, which utilizes dielectric materials with high permittivity, plays a crucial role in preserving the surface charge generated via triboelectrification. This preservation is achieved through a coupling effect that involves both electron blocking and enhanced polarization mechanisms.[9] Furthermore, there is ongoing research on incorporating blocking-trapping-multi-interlayers[10] and developing microcapacitors[11] within TENG structures. It is worth noting that an essential characteristic emphasized in earlier studies regarding TENG interlayer materials revolves around their significant charge storage capacity. The primary goal is to mitigate charge decay and enhance the overall performance of TENG systems.

Considering the capability of charge storage capacity, the electric double layer (EDL) formed by ions has demonstrated a superior charge storage capacity which can be employed to supercapacitors. There have been several attempts to employ the EDL in TENGs, such as embedding ions into the charge collecting layer or electrification layer,[12] connecting ion gel capacitors to TENG,[13] and applying the EDL effect via a 3-layer structure.[14] Although ionic liquid-based EDL has yet to be considered as an intermediate layer, its incorporation holds the potential to reduce triboelectric charge decay with high charge capacity. Furthermore, ionic liquids can be impregnated in various materials

D. U. Lim, E. J. Lee, J. K. Jang, S. Kim, S. Y. Lee, T.-H. Kim
Division of Advanced Materials
Korea Research Institute of Chemical Technology (KRICT)
Daejeon 34114, Republic of Korea
E-mail: sylee@krict.re.kr; thkim@krict.re.kr

S. Y. Lee
Advanced Materials and Chemical Engineering
University of Science and Technology (UST)
Daejeon 34113, Republic of Korea

The ORCID identification number(s) for the author(s) of this article can be found under https://doi.org/10.1002/adfm.202401717

DOI: 10.1002/adfm.202401717

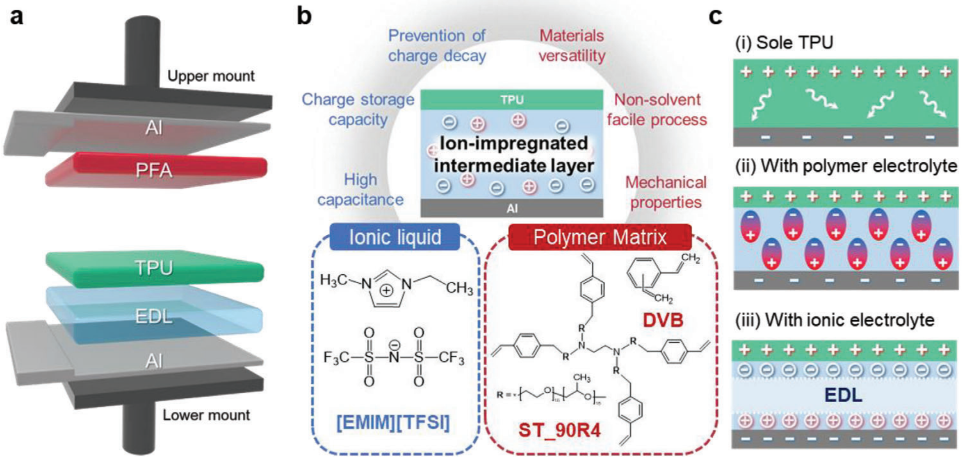

Figure 1. The structure and characteristics of the iEDL-TENG a) Schematic structure and b) materials characteristic of iEDL-TENG. c) Schematic representation of the effect resulting from iEDL insertion in the conventional TENG structure.

such as polymers and hydrogels, enabling their versatile synthesis and the potential for achieving high mechanical properties. Many previous studies have primarily focused on the electrical performance of TENG, often overlooking its mechanical properties. However, sacrificing mechanical properties in favor of improved TENG output performance could limit its potential for use in diverse IoT and flexible biological devices. Hence, incorporating an EDL layer based on ionic liquids into TENG represents a favorable approach to boost output performance without compromising mechanical durability by reducing triboelectric charge decay. Furthermore, materials used in earlier studies, including 2D materials and nanoparticles, encounter issues such as not only compromised mechanical characteristics but also high costs, limited sustainability, and complex manufacturing processes. In contrast, the ionic layer, which can be tailored with various materials, emerges as a promising solution for TENG interlayer materials. This approach facilitates straightforward manufacturing procedures, cost-efficiency, and stability.

In this study, we present a TENG structure incorporating an ionic EDL as an intermediate layer to counteract undesirable charge decay. To enable the incorporation of EDL as the intermediate layer in TENG, we enhanced the mechanical stability of the conventional ionic electrolyte through cross-linking. Our solvent-free-cross-linking process is compatible with various substances, and we selected mechanically stable thermoplastic polyurethane (TPU) as the triboelectrificating layer for TENG fabrication. Furthermore, by using the commercially available and widely used polyethylene oxide (PEO) and polypropylene oxide (PPO)-based non-ionic polymeric surfactant as an electrolyte polymer, both the cost and stability concerns can be effectively addressed. Consequently, with the incorporation of ionic EDL, a significant enhancement in current density (10–92 mA m^{-2}) is observed compared to the marginal increment in the voltage output (≈200–280 V), suggesting the improved efficiency in charge transfer rather than facilitating charge generation from triboelectrification. Our findings indicate that the reduction in charge decay via the intermediate layer was facilitated primarily by the availability of ions, regardless of the implemented electrolyte polymer. This result is speculated to be related to the high capacitance (4.75 μF cm^{-2}) of the ionic EDL. Furthermore, the mechanically stable TENG with the incorporated EDL exhibited stable performance even after 10,000 operational cycles and maintained its performance against severe crumpling and injury from a blade. Based on the high power density (26 W m^{-2}) and stability of ionic-EDL-TENG, we demonstrated its ability to power 100 commercial LEDs and TENG-charged capacitors

2. Results and Discussion

Figure 1a presents a schematic of the TENG structure with an ion-impregnated intermediate layer inserted to induce an ionic EDL (iEDL-TENG). In this setup, perfluoroalkoxy alkane (PFA) and TPU were utilized as materials for the triboelectrification layer. Additionally, Al was utilized for charge collection. The ultraviolet (UV) curable ion-impregnated intermediate layer, inserted between TPU and Al electrode, comprised of electrolyte polymer (ST_90R4) and cross-linker (Divinylbenzene, DVB). We incorporated the well-known commercial ionic liquid 1-Ethyl-3-methylimidazolium bis(trifluoromethylsulfonyl)imide, denoted as [EMIM][TFSI], into this layer. A schematic of the detailed fabricating process is illustrated in Figure S1 (Supporting Information). [EMIM][TFSI] can have high capacitance by forming EDL in TENG, enabling prevent charge decay (Figure 1c). Our choice of ST_90R4, designed with vinyl end groups, facilitates easy cross-linking. This liquid-state mixture, when combined with the cross-linker DVB, enables compatibility with a wide range of materials, owing to the solvent-free process, as illustrated in Figure 1b.

The TENG interlayer material ST_90R4 was synthesized by substituting the end groups of Tectronic90R4 (which is a PEO and PPO-based copolymer and used as a non-ionic polymeric surfactant) with vinyl groups. Confirmation of the substituted vinyl groups was achieved through nuclear magnetic resonance (NMR) spectroscopy (Figure S2, Supporting Information). By combining the liquid-state ST_90R4 with the liquid cross-linker DVB, an[EMIM][TFSI], along with a small quantity of photoinitiator, and subjecting this mixture to UV light exposure, the solution can be solidified to serve as an iEDL layer (as depicted in **Figure** 2a). Further details regarding the chemical reaction can be

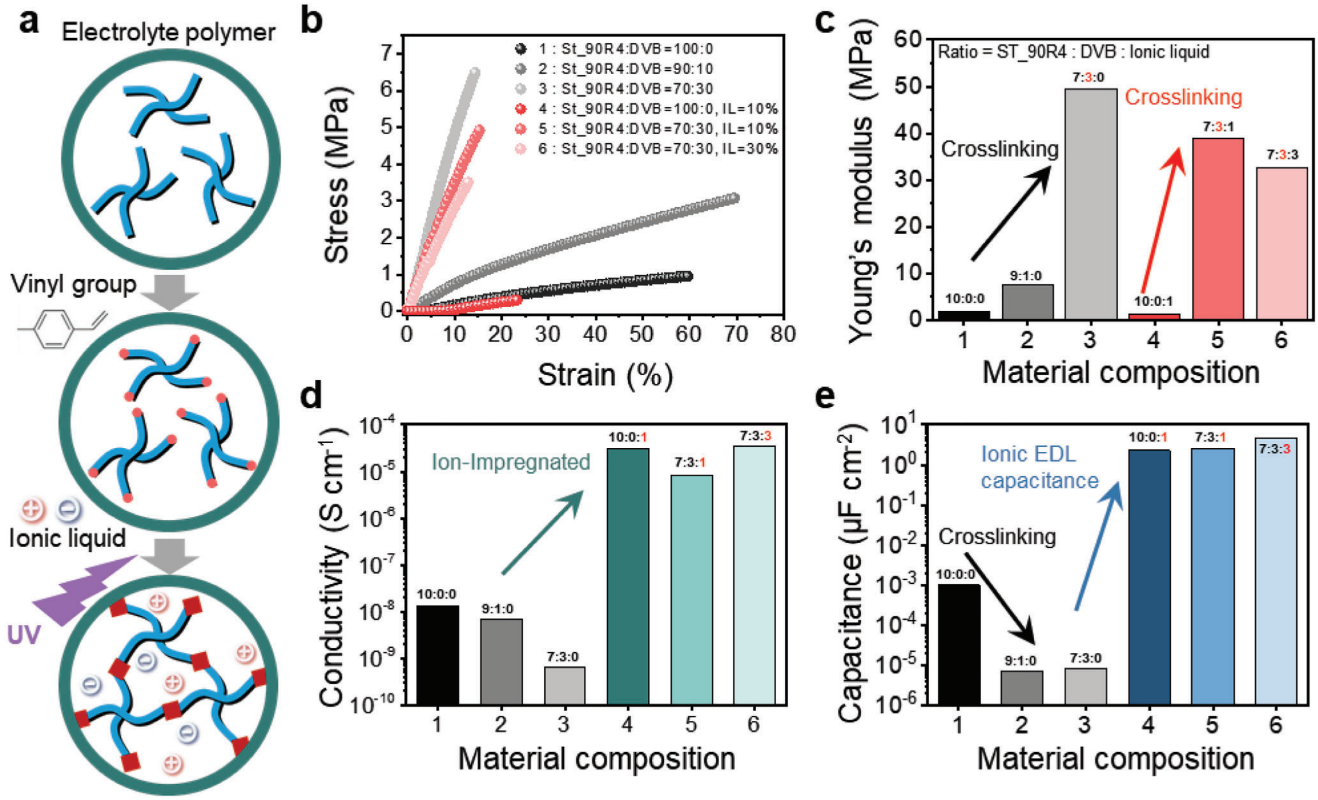

Figure 2. Synthesis and characteristics of the ionic intermediate layer. a) Schematic illustrations of ST_90R4 synthesis. b) Stress-strain curve, c) Young's modulus, d) conductivity, and (e) capacitance of the compositionally graded ionic intermediate layer (ST_90R4:DVB:Ionic liquid).

found in Figure S3 (Supporting Information). Figure 2b,c provide insight into the mechanical properties of ST_90R4 as they vary with different ratios of DVB and ionic liquid. It is evident from Figure 2a,b that the mechanical strength of ST_90R4 experiences a significant increase when the DVB ratio exceeds 30%. The addition of the ionic liquid has a minor reducing effect on mechanical strength. Notably, the results involving DVB incorporation include UV exposure during the process. The high rigidity, indicated by the high Young's modulus, enables TENG to maintain stable operation even under high pressure during energy harvesting measurements. Figure 2d shows the conductivity data. The incorporation of DVB increases resistance due to its cross-linking effect (depicted by the black-gray bars). However, even with just a 10% addition of ionic liquid compared to ST_90R4, conductivity improves by more than 1,000 times (green bars). This indicates that the ionic liquid can move freely within ST_90R4, contributing to the significant improvement in conductivity. Although the addition of DVB hampers the movement of the ionic liquid due to cross-linking, raising the ionic liquid concentration to ≈30% compared to ST_90R4 is sufficient to overcome this issue, as shown by the results. One point to note is that the conductivity solely within the iEDL does not represent the overall resistance of the device. Typically, due to the high interfacial resistance between layers, the high conductivity of the iEDL does not assist in increasing leakage current in TENGs. In terms of capacitance measurements (as indicated by the black-gray bars in Figure 2e), it is evident that the incorporation of DVB, which induces cross-linking, interferes with the induced dipole effect. This interference results in a decrease in the dielectric constant and consequently leads to lower capacitance. However, with the addition of the ionic liquid, a significantly higher capacitance induced by the iEDL is observed, irrespective of the cross-linking induced by DVB. The high capacitance of the ionic liquid, within the range of 4.75 μF cm^{-2}, bestows it with a substantial charge storage capacity. The capacitance of the ionic interlayer is more than 20 times higher than the capacitance of TiO_x (Table S1, Supporting Information), a high k dielectric used as a charge blocking layer.[8] Consequently, it can effectively prevent the dissipation of accumulated charges resulting from triboelectrification.

Figure 3a demonstrates that a structure containing only the conventional triboelectrification layer experiences reduced charge, influenced by susceptibility to charge recombination. As shown in the figure, however, incorporating an iEDL layer results in a remarkable reduction in charge recombination, allowing higher currents to flow. Figure 3b–d presents the performance characteristics of bare TENG structure, interlayer structure with only electrolyte, and interlayer structure with ionic liquid-impregnated layer. Figure 3b shows no significant increase in the output voltage. However, Figure 3c,d highlights the exceptional performance improvements achieved by the iEDL-TENG: a nearly 10-fold increase in current density (92 mA m^{-2}), leading to a 13-fold increase in power density (26 W m^{-2}). The key factor contributing to this enhanced performance is EDL formation. Nevertheless, when considering practical TENG measurements, the critical aspect in device fabrication lies in the synthesis of ST_90R4, which serves as a stable electrolyte matrix.

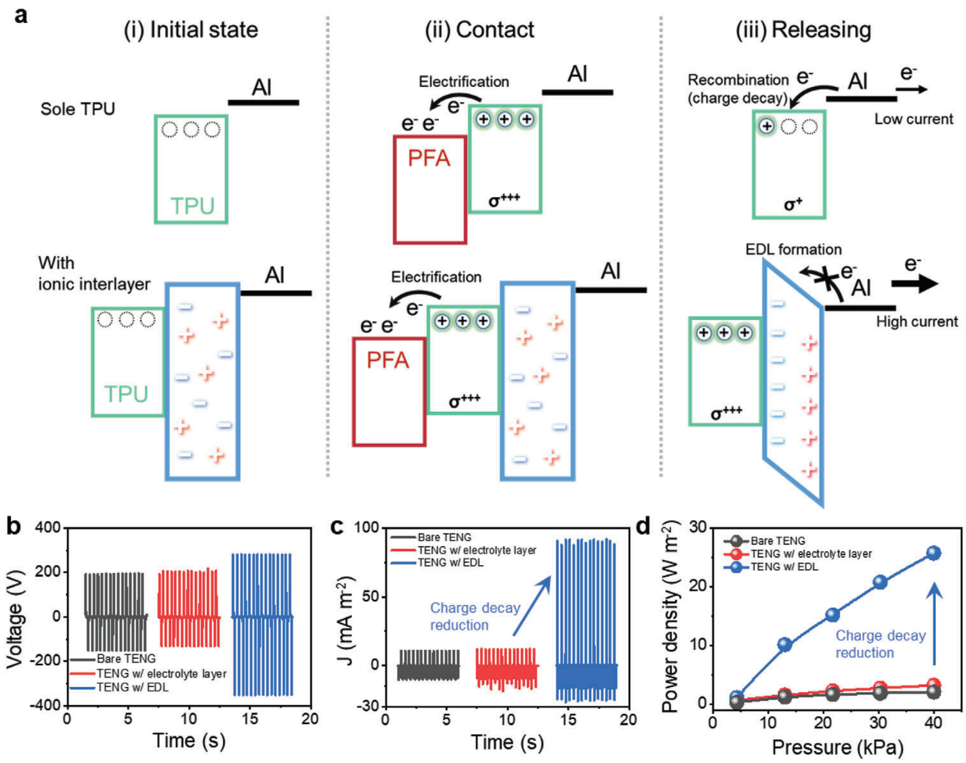

Figure 3. Principle and characteristics of the iEDL-TENG a) The principle of charge decay reduction of ionic interlayer based on band diagram. b) The output voltage, c) the output current density, and d) power density of various TENG structures.

As depicted in Figure 3b–d, the incorporation of iEDL as a TENG interlayer resulted in a significant increase in current density rather than voltage. This phenomenon can be attributed to the charge decay prevention effect of iEDL. Surface charge measurements were taken to further validate the enhancement in charge decay. **Figure** 4a, demonstrates that the presence or absence of iEDL is correlated with the amount of surface charge. The notably higher increase in current compared to surface charge and voltage is noteworthy. We speculate that the higher increase in current compared to other factors is due to the decreased internal resistance of the device. Particularly, we anticipate that the interfacial resistance between each layer, which is expected to be the highest within the device, has decreased. This is attributed to the characteristic of the iEDL, where the ionic liquid can move freely, potentially forming liquid-solid interfaces rather than solid-solid interfaces. This hypothesis underscores the need for further research and in-depth discussion on interfacial properties. Figures, 4b,c illustrate the output voltage and current density of iEDL-TENG at varying ionic liquid contents within iEDL, aiming to identify the optimal output conditions. As the ratio of ionic liquid to ST_90R4 increases, the output performance of iEDL-TENG improves, peaking at ≈30%. Beyond this point, performance starts to decline. The deterioration in performance beyond a specific ratio (>30%) can be attributed to the increased quantity of ionic liquid, resulting in reduced mechanical rigidity and less favorable TENG measurements (specifically, in the vertical contact-separation mode employed in this study). Furthermore, the amount of voltage variation gradually decreases as the pressure increases. However, the current density exhibits a close-to-linear variation with increasing pressure. The behavior of voltage and current density is explained in terms of the relative current, represented as relative current = output current/voltage, as shown in Figure 4d.

It is evident that both the bare TENG structure and the dielectric interlayer structure without ionic liquid exhibit a decrease in voltage-to-current efficiency at high voltages. This decrease is a common phenomenon that occurs as accumulated charge increases, leading to a higher loss rate. However, in the presence of ionic liquid, the voltage-to-current efficiency increases at high pressures. This phenomenon can be attributed to the higher surface charge, resulting in a greater amount of charge being lost before reaching the charge-collecting layer. By forming the iEDL, losses can be minimized and efficiency can be enhanced, as demonstrated in Figure 4e. The observed difference is speculated to be primarily due to charge recombination becoming the main factor in charge decay as more charge is generated. In our measurement environment, the distance between the two charge layers remains constant, thus limiting the impact of air breakdown. Therefore, it is conjectured that with the generation of a significant amount of charge, the proportion of charge recombination in charge decay becomes higher. As a result, preventing charge recombination leads to higher currents being measured compared to voltage at high pressure (= high charge generation).

Another essential feature of iEDL-TENG is its remarkable mechanical stability, which ensures consistent and reliable performance throughout its operation. The iEDL layer effectively mitigates charge decay in direct proportion to the area it occupies, regardless of direct contact between the dielectric (TPU) and charge

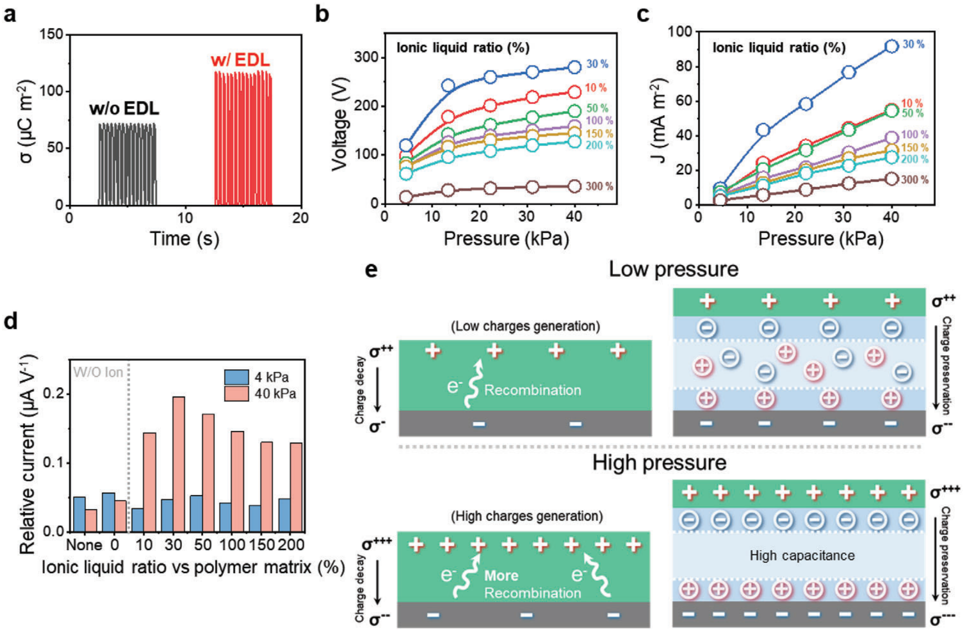

Figure 4. Output performance and mechanism of iEDL-TENG operation. a) Surface charge density (σ) with and without the iEDL. b) Output voltage and c) output current density as a function of applied pressure to iEDL-TENG. d) Ratio of the output current and voltage (I/V) at low pressure (blue) and high pressure (red). e) Schematic depicting the mitigation of charge decay in the iEDL.

collecting (Al) layers. As shown in **Figure 5a**, the output performance of the device varies proportionally with the area (0, 2 and 6 cm^2) of the iEDL interlayer in the component. It is deemed that a proportional relationship based on the area likely arises from differences in charge storage capacity between the layers. Hence, even if the TENG component is damaged or short circuited due to physical forces, the iEDL remains unaffected and continues to function properly. This explains the stable performance observed during 10,000 operational cycles, shown in Figure 5b. The peak output voltages during the 10,000 cycles show a significantly small standard deviation of ≤0.1 V. iEDL-TENG exhibits not only excellent stability during continuous operation but also remarkable resilience against external physical forces. Figures 5c,d show the performance of the iEDL-TENG after being subjected to blade-induced cuts, penetrating wounds, and severe crumpling. The process of applying physical force was recorded in a 1-take video (Movie S1, Supporting Information). It was observed that after inflicting cutting and penetrating wounds, the output current increased. This is attributed to the fact that the damage to the device did not cause a decrease in performance, and the increased surface roughness led to a larger amount of charge being accumulated, resulting in an enhanced output current. Compared to interlayer materials with poor mechanical properties, it is worth highlighting that iEDL's ability to maintain stable performance even under external forces, such as cracks and shorts, is attributed to its independence and resilience in such situations.

The iEDL-TENG demonstrates superior charge transfer efficiency and mechanical stability, making it a strong candidate for practical applications. **Figure 6a** and Movie S2 (Supporting Information) show the operation of 100 green LEDs without energy storage. We verified that the high-power iEDL-TENG can charge capacitors of various capacities ranging from 4.7 to 470 μF, as shown in Figure 6d. Power measurements, presented in Figure 6b, were obtained by incorporating different load resistors ranging from 1 MΩ to 3 GΩ. The capability to charge high-capacity capacitors indicates the potential for broad application of iEDL-TENG in various scenarios. Particularly in IoT systems, where electronic devices are dispersed among various objects, the use of eco-self-powered devices such as TENG can be a suitable approach. Self-powered devices with high power output and mechanical stability, such as iEDL-TENG, are expected to have significant value for various IoT applications, including wearable devices and sensor networks in smart houses.

3. Conclusion

In summary, we reported a TENG structure with high mechanical stability and high output performance, achieved through the utilization of an ion-containing electrolyte as an interlayer. This novel approach involved the modification of a low-cost PEO-PPO-based copolymer with vinyl groups, enabling the solvent-free blending of ionic liquid and a cross-linker, ultimately achieved through UV exposure. The resulting iEDL-TENG, featuring a robust mechanical profile and high capacitance, exhibited a remarkable tenfold increase in current density, reaching 92 mA m^{-2}, when compared to devices without the iEDL layer. In particular, the power density increased by 13 times, reaching 26 W m^{-2}. The increase in current per voltage with applied pressure suggests that the iEDL layer primarily improves charge transfer efficiency, rather than solely contributing to charge generation. Furthermore, the mechanically stable iEDL-TENG consistently delivered outstanding output performance even after undergoing 10,000 operational cycles. It exhibited minimal degradation in performance when subjected to blade scratches, penetrations, and severe crumpling. Impressively, one iEDL-TENG device can effectively power 100 LEDs and efficiently

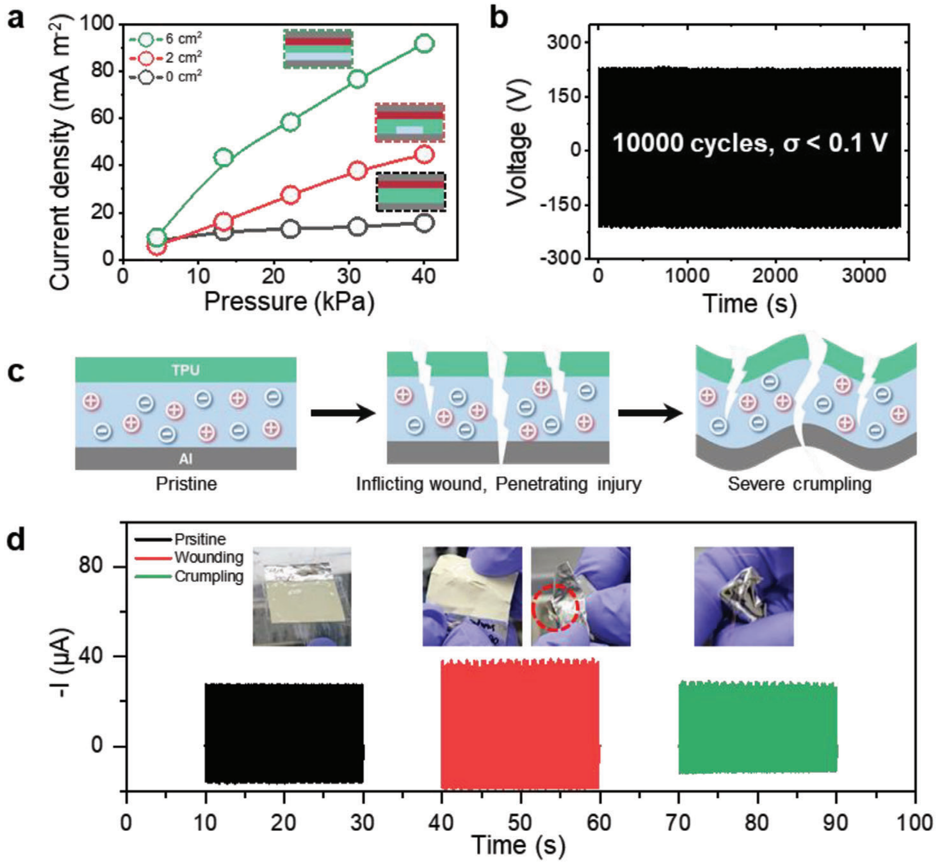

Figure 5. Durability and mechanical stability of the iEDL-TENG. a) Current density for different ionic intermediate layer area sizes. b) Cyclic operating test of the iEDL-TENG. c) Schemes and d) output current of the iEDL-TENG corresponding to various physical defects.

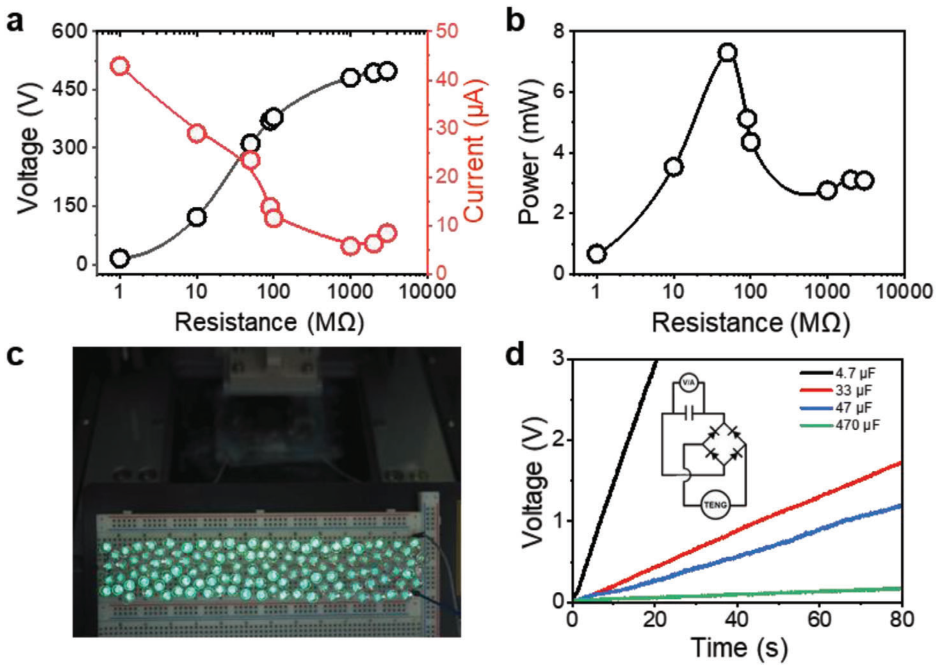

Figure 6. iEDL-TENG applications. a) Output open-circuit voltage, short-circuit current and b) output power under variable external load resistances. c) Photograph of 100 LEDs operated by the iEDL-TENG. d) Charge voltage in various capacitors.

charge a 470 µF capacitor. This implementation of an ionic-interlayer represents a significant milestone, paving a stable and cost-effective path to enhance TENG efficiency by minimizing charge decay.

4. Experimental Section

Synthesis of ST_90R4: A total of 50 g of ethylenediamin tetrakis (ethoxylate-block-propoxylate) tetrol (Tectronic 90R4, Mn ≈7200, Sigma–Aldrich), which was dried under vacuum at room temperature overnight, and 2.22 g of sodium hydride (NaH, 60% dispersion in mineral oil, Sigma–Aldrich) were dissolved in 360 ml of Tetrahydrofuran (THF, anhydrous, Sigma–Aldrich) in a 3-neck brown flask. The mixture of 7.3 mL of 4-Vinylbenzyl chloride (VBC, 90%, Sigma–Aldrich) and 10 mL of THF were added dropwise to the solution using a syringe. After stirring for 48 h in an argon gas environment at a temperature not exceeding 40 °C, THF was removed using a vacuum evaporator. The mixture without THF was dissolved in 500 ml of methylene chloride (MC, Extra pure grade, Duksan) and mixed with 500 mL of saturated NaCl solution in a separating funnel to discard the NaCl portion. After three repetitions, the solution was subjected to vacuum filtration using a qualitative filter paper (Hyundai Micro). The filtered solution was subjected to vacuum distillation, followed by precipitation in petroleum ether (GR grade, Duksan), and the resulting mixture was separated from petroleum ether using a separating funnel. The separated solution was filtered through a 1 µm filter paper (Merck Millipore Ltd.) using ≈50 mL of THF, followed by vacuum distillation. The remaining solution was then removed using a vacuum oven to obtain ST_90R4.

Fabrication of iEDL-TENG: ST_90R4 and DVB were mixed in a weight ratio of 7:3, and then [EMIM][TFSI](C-TRI) was added according to the target ratio. The photo-initiator, phenylbis(2,4,6-trimethylbenzoyl) phosphine oxide (97%, Sigma–Aldrich), and diphenyl (2,4,6 – trimethylbenzoyl) phosphine oxide (97%, Sigma–Aldrich), were added in a 1:1 ratio, constituting ≈3% of the total solution weight. The prepared ionic solution was coated onto TPU and then evenly spread on hydrophobic-coated polyethylene terephthalate film followed by UV exposure. An Al foil was attached over the cured ionic layer. The PFA film attached to the Al foil serves as the counter triboelectrification layer.

Characterization and Measurements: The degree of substitution and synthesis of ST_90R4 were determined using NMR spectroscopy. The output voltage measured in the TENG was recorded using an oscilloscope (MDO 34 3-BW-200, Tektronix), and the output current was converted to voltage using a low-noise current preamplifier (SR570, Stanford Research Systems, Inc.) before oscilloscope measurement.

Supporting Information

Supporting Information is available from the Wiley Online Library or from the author.

Acknowledgements

This research was supported by the Korea Research Institute of Chemical Technology (KRICT, KS2422-10, KS2421-10) and the National Research Foundation (NRF) grant funded by the Korean Government (NRF-2021M3D1A2043793).

Conflict of Interest

The authors declare no conflict of interest.

Author Contributions

T.-H.K. and S.Y.L. conceived the idea and initiated the project. D.U.L. and E.J.L. performed the fabrication, optimization, and characterization of materials and devices. D.U.L. conducted the physical interpretations of the materials and device data. D.U.L. wrote the manuscript. J.K.J. and S.K. contributed to the material synthesis and optimizations. T.-H.K. and S.Y.L. supervised the project. All the authors read and commented on the manuscript.

Data Availability Statement

The data that support the findings of this study are available in the supplementary material of this article.

Keywords

charge capacitance, charge decay, electrolyte polymers, ionic liquid, triboelectric nanogenerators

Received: January 29, 2024
Revised: April 15, 2024
Published online:

[1] F.-R. Fan, Z.-Q. Tian, Z. L. Wang, *Nano Energy* **2012**, *1*, 328.
[2] a) W.-G. Kim, D.-W. Kim, I.-W. Tcho, J.-K. Kim, M.-S. Kim, Y.-K. Choi, *ACS Nano* **2021**, *15*, 258; b) A. Ahmed, I. Hassan, M. F. El-Kady, A. Radhi, C. K. Jeong, P. R. Selvaganapathy, J. Zu, S. Ren, Q. Wang, R. B. Kaner, *Adv. Sci.* **2019**, *6*, 1802230; c) Z. L Wang, *Mater. Today* **2022**, *52*, 348.
[3] a) K. Dong, Z. Wu, J. Deng, A. C. Wang, H. Zou, C. Chen, D. Hu, B. Gu, B. Sun, Z. L. Wang, *Adv. Mater.* **2018**, *30*, 1804944; b) X. Wang, W.-Z. Song, M.-H. You, J. Zhang, M. Yu, Z. Fan, S. Ramakrishna, Y.-Z. Long, *ACS Nano* **2018**, *12*, 8588; c) Z. H. Guo, H. L. Wang, J. Shao, Y. Shao, L. Jia, L. Li, X. Pu, Z. L. Wang, *Sci. Adv.* **2022**, *8*, eabo5201; d) C. Ye, D. Liu, P. Chen, L. N. Cao, X. Li, T. Jiang, Z. L. Wang, *Adv. Mater.* **2023**, *35*, 2209713; e) C. Wang, P. Wang, J. Chen, L. Zhu, D. Zhang, Y. Wan, S. Ai, *Nano Energy* **2022**, *93*, 106828; f) Z. Zhou, P. Wang, J. Li, C. Wang, J. Chen, L. Zhu, H. Zhu, D. Zhang, *Nano Energy* **2022**, *98*, 107317; g) Z. L. Wang, *Adv. Energy Mater.* **2020**, *10*, 2000137.
[4] a) L. Zhao, Q. Zheng, H. Ouyang, H. Li, L. Yan, B. Shi, Z. Li, *Nano Energy* **2016**, *28*, 172; b) T. Bhatta, P. Maharjan, H. Cho, C. Park, S. H. Yoon, S. Sharma, M. Salauddin, M. T. Rahman, S. S. Rana, J. Y. Park, *Nano Energy* **2021**, *81*, 105670; c) J. Xu, Y. Zou, A. Nashalian, J. Chen, *Frontiers in Chemistry* **2020**, *8*, 577327; d) Y. Liu, W. Liu, Z. Wang, W. He, Q. Tang, Y. Xi, X. Wang, H. Guo, C. Hu, *Nature Commun.* **2020**, *11*, 1599; e) P. Cheng, H. Guo, Z. Wen, C. Zhang, X. Yin, X. Li, D. Liu, W. Song, X. Sun, J. Wang, *Nano Energy* **2019**, *57*, 432; f) H.-J. Choi, J. H. Lee, J. Jun, T. Y. Kim, S.-W. Kim, H. Lee, *Nano Energy* **2016**, *27*, 595; g) Y. Zou, J. Xu, K. Chen, J. Chen, *Adv. Mater. Technol.* **2021**, *6*, 2000916.
[5] a) Y. Zi, S. Niu, J. Wang, Z. Wen, W. Tang, Z. L. Wang, *Nat. Commun.* **2015**, *6*, 8376; b) C. Wang, H. Guo, P. Wang, J. Li, Y. Sun, D. Zhang, *Adv. Mater.* **2023**, 2209895; c) N. Cui, L. Gu, Y. Lei, J. Liu, Y. Qin, X. Ma, Y. Hao, Z. L. Wang, *ACS Nano* **2016**, *10*, 6131.
[6] X. Xie, X. Chen, C. Zhao, Y. Liu, X. Sun, C. Zhao, Z. Wen, *Nano Energy* **2021**, *79*, 105439.
[7] a) J.-K. Kim, G. H. Han, S.-W. Kim, H. J. Kim, R. Purbia, D.-M. Lee, J. K. Kim, H. J. Hwang, H.-C. Song, D. Choi, *Energy Environ. Sci.* **2023**; b) S. Cui, L. Zhou, D. Liu, S. Li, L. Liu, S. Chen, Z. Zhao, W. Yuan, Z. L. Wang, J. Wang, *Matter* **2022**, *5*, 180; c) D. W. Kim, J. H. Lee, I. You, J. K. Kim, U. Jeong, *Nano Energy* **2018**, *50*, 192; d) S. Lv, X. Zhang, T. Huang, H. Yu, Q. Zhang, M. Zhu, *ACS Appl. Mater. Interfaces* **2021**, *13*, 2566; e) Y. Nan, X. Wang, H. Xu, Y. Wu, H. Zhou, Y. Sun, T. Yu, Y. Huang, *Nano Energy* **2023**, *110*, 108345; f) X. Chen, Y. Liu, Y. Sun, T.

Zhao, C. Zhao, T. A. Khattab, E. G. Lim, X. Sun, Z. Wen, *Nano Energy* **2022**, *98*, 107236.
[8] H.-W. Park, N. D. Huynh, W. Kim, C. Lee, Y. Nam, S. Lee, K.-B. Chung, D. Choi, *Nano Energy* **2018**, *50*, 9.
[9] a) J. Wang, C. Wu, Y. Dai, Z. Zhao, A. Wang, T. Zhang, Z. L. Wang, *Nat. Commun.* **2017**, *8*, 88; b) P.-C. Lee, Y.-C. Ou, R.-C. Wang, C.-P. Liu, *Nano Energy* **2021**, *89*, 106394.
[10] a) N. Cui, J. Liu, Y. Lei, L. Gu, Q. Xu, S. Liu, Y. Qin, *ACS Appl. Energy Mater.* **2018**, *1*, 2891; b) Z. Li, M. Zhu, Q. Qiu, J. Yu, B. Ding, *Nano Energy* **2018**, *53*, 726; c) H. Jiang, H. Lei, Z. Wen, J. Shi, D. Bao, C. Chen, J. Jiang, Q. Guan, X. Sun, S.-T. Lee, *Nano Energy* **2020**, *75*, 105011.
[11] a) J. Chun, J. W. Kim, W.-s. Jung, C.-Y. Kang, S.-W. Kim, Z. L. Wang, J. M. Baik, *Energy Environ. Sci.* **2015**, *8*, 3006; b) X. He, H. Guo, X. Yue, J. Gao, Y. Xi, C. Hu, *Nanoscale* **2015**, *7*, 1896; c) Z. Zhang, Y. Xu, D. Wang, H. Yang, J. Guo, L.-S. Turng, *Nano Energy* **2019**, *60*, 903.
[12] a) Y. Liu, C. Zhao, Y. Xiong, J. Yang, H. Jiao, Q. Zhang, R. Cao, Z. L. Wang, Q. Sun, *Adv. Funct. Mater.* **2023**, 2303723; b) Y. Lee, S. H. Cha, Y.-W. Kim, D. Choi, J.-Y. Sun, *Nat. Commun.* **2018**, *9*, 1804; c) T. Liu, M. Liu, S. Dou, J. Sun, Z. Cong, C. Jiang, C. Du, X. Pu, W. Hu, Z. L. Wang, *ACS nano* **2018**, *12*, 2818; d) X. Pu, M. Liu, X. Chen, J. Sun, C. Du, Y. Zhang, J. Zhai, W. Hu, Z. L. Wang, *Sci. Adv.* **2017**, *3*, e1700015; e) H. J. Hwang, J. S. Kim, W. Kim, H. Park, D. Bhatia, E. Jee, Y. S. Chung, D. H. Kim, D. Choi, *Adv. Energy Mater.* **2019**, *9*, 1803786.
[13] J. H. Lee, Y. S. Park, S. Cho, I. S. Kang, J. K. Kim, U. Jeong, *Nano Energy* **2018**, *54*, 367.
[14] J. Chun, B. U. Ye, J. W. Lee, D. Choi, C.-Y. Kang, S.-W. Kim, Z. L. Wang, J. M. Baik, *Nat. Commun.* **2016**, *7*, 12985.

